Interaction between buoyancy and diffusion-driven instabilities of propagating autocatalytic reaction fronts. I. Linear stability analysis

J. D'Hernoncourt,[1] J. H. Merkin,[2,a)] and A. De Wit[1]
[1]*Nonlinear Physical Chemistry Unit and Center for Nonlinear Phenomena and Complex Systems, Faculté des Sciences, Université Libre de Bruxelles (ULB), CP 231-Campus Plaine, 1050 Brussels, Belgium*
[2]*Department of Applied Mathematics, University of Leeds, Leeds LS2 9JT, United Kingdom*

(Received 18 August 2008; accepted 9 January 2009; published online 17 March 2009)

The interaction between buoyancy-driven and diffusion-driven instabilities that can develop along a propagating reaction front is discussed for a system based on an autocatalytic reaction. Twelve different cases are possible depending on whether the front is ascending or descending in the gravity field, whether the reactant is heavier or lighter than the products, and whether the reactant diffuses faster, slower, or at the same rate as the product. A linear stability analysis (LSA) is undertaken, in which dispersion curves (plots of the growth rate σ against wave number k) are derived for representative cases as well as an asymptotic analysis for small wave numbers. The results from the LSA indicate that, when the initial reactant is denser than the reaction products, upward propagating fronts remain unstable with the diffusion-driven instability enhancing this instability. Buoyantly stable downward propagating fronts become unstable when the system is also diffusionally unstable. When the initial reactant is lighter than the reaction products, any diffusionally unstable upward propagating front is stabilized by small buoyancy effects. A diffusional instability enhances the buoyant instability of a downward propagating front with there being a very strong interaction between these effects in this case. © *2009 American Institute of Physics*. [DOI: 10.1063/1.3077180]

I. INTRODUCTION

Propagating reaction-diffusion fronts can become unstable to transverse perturbations in two essentially different ways. There can be density gradients across the reaction front caused by the changes in the reactant concentrations, which can lead to a buoyantly unstable configuration. For example, in the iodate-arsenous acid (IAA) reaction in the arsenous acid (AA) excess case,[1–8,49] the iodide-nitric acid[9] and iodate-sulfite reactions,[10,11] as well as commonly in combustion fronts,[12,13] the products of the reaction, are less dense than the unreacted state. Thus any isothermal reaction front propagating in an upward direction will be buoyantly unstable, while the downward propagating one remains stable and planar. The opposite is the case for other families of reactions[14] such as the chlorite-tetrathionate (CT),[15–23] nitric acid-iron(II),[24–26] reactions, or polymerization fronts.[50,51] Here, in isothermal conditions, the reaction products are denser and so a downward propagating front will be buoyantly unstable featuring density fingering while the upward moving front remains stable.

An alternative way for reaction-diffusion fronts to become unstable is through the diffusion coefficients of the substrate and autocatalyst being sufficiently different. This can lead to a diffusion-driven instability.[27–35] This has been established theoretically for the cubic autocatalytic reaction[27,28,35]

$$A + 2B \rightarrow 3B \quad \text{rate } k_0 ab^2, \tag{1}$$

for example, where a and b are, respectively, the concentrations of reactant A and autocatalyst B and k_0 is a kinetic constant. This cubic scheme has been shown to be a good approximation for the IAA reaction in the AA-excess case[36] with $A \equiv IO_3^-$ and $B \equiv I^-$, and for which cellular deformation due to a diffusive instability has been observed experimentally.[29] For this case, if $D = D_B/D_A < D_c$, with $D_c \simeq 0.424$, a planar reaction front becomes diffusionally unstable.[28,35] A similar situation arises in the CT system where diffusive instabilities have been studied experimentally in detail,[31,32,34] where the critical diffusion coefficient ratio needed in a two-variable model[32,33] for this reaction is now $D_c \simeq 0.45$.

As the same autocatalytic chemical fronts can feature either a hydrodynamic buoyancy-driven fingering due to a Rayleigh-Taylor (RT) mechanism or cellular deformation due to a diffusive instability, our goal is to analyze whether these two different instabilities can interact and, if so, what will be the resulting dynamics. As well we also wish to understand in general the influence of simple differential diffusion between the two key species of an autocatalytic reaction on the RT instability even in the absence of diffusive instability (i.e., $D > D_c$ but $D \neq 1$).

Previous work on a model for the isothermal CT system has already shown that increasing D above unity has a stabilizing effect on the RT instability of descending fronts.[37,38] In a similar way, differential diffusion between mass and heat, i.e., the two key variables in exothermic traveling fronts, has previously been shown to affect the stability properties and nonlinear dynamics of exothermic autocatalytic

a)Electronic mail: amtjhm@maths.leeds.ac.uk.

fronts in aqueous solutions (see Refs. 16, 39, and 40, and references therein). However, in these exothermic autocatalytic frontal systems, the evolution equation for the temperature T depends explicitly on the concentration c, while changes in T do not feedback on the dynamics of the concentration since the temperature changes across the front are only of the order of 1 K. The coupling between the effects of the two key species is therefore not the same as the one operative for a chemical scheme such as Eq. (1), where each species A and B has a feedback on the other. For combustion fronts, the interaction between diffusive and RT instabilities has been addressed and has been shown to yield to modified dispersion curves and complex dynamics such as periodic or irregular pulsating flames.[42] However in such systems, temperature changes are large enough to affect the kinetic constant. This is only a second-order effect for autocatalytic reactions in aqueous solutions, where the temperature changes across the front are usually in the range of 0.5–2 K.

In this framework it is the objective of this article to study theoretically the stability properties that result from the coupling between RT instabilities and the differential diffusion of the reactant and autocatalyst species involved in an isothermal traveling chemical front. To do so, we consider reaction (1) as a prototype system to model generic autocatalytic fronts. In particular, we concentrate on those parameter ranges where the different mechanisms for generating a transverse instability (RT or diffusive instabilities) have comparable effects. We set up the model and nondimensionalization of the problem, seek traveling wave solutions as a base state to the problem and perform a linear stability analysis (LSA) by deriving dispersion curves (giving the growth rate of the perturbations as a function of their wave number) for representative values of the parameters. Numerical simulations of the full nonlinear problem are discussed in a following paper.[43]

We find as a result of the LSA that the problem can be classified into 12 different cases depending whether the density increases or decreases across the front, whether the front is ascending or descending in the gravity field, and whether $D=1$, $D>1$, or $D<1$. In order to demonstrate this, the present article is organized as follows. In Sec. II, we introduce a two-variable reaction-diffusion-convection model based on the reaction scheme (1) for species A and B diffusing at different rates and coupled to Darcy's law to describe the evolution of the flow field in the system. The LSA is detailed in Sec. III, where we also consider an analysis for small wave numbers. Finally we draw some conclusions in Sec. IV.

II. MODEL

Our model is based on reaction scheme (1) taking place within a porous medium or a thin Hele–Shaw cell. This choice of geometry is made, in part, because a Hele–Shaw setup has been used in many experimental studies into the instabilities of reaction fronts and because it simplifies, to some extent, the basic fluid dynamics. In the latter regard, it allows for the assumption that the system is effectively two-dimensional. We assume that the Hele–Shaw reactor is mounted in the vertical direction, with the x-axis measuring distance in the upward direction and y normal to x across the cell. The equations for our two-dimensional model system are derived from the standard thin film equations (lubrication theory) (see Ref. 44 for example) for the fluid flow together with reaction-diffusion-advection equations for the concentrations, also derived using the thin film approximation, namely,

$$\frac{\partial u}{\partial x}+\frac{\partial v}{\partial y}=0, \tag{2}$$

$$\frac{\partial p}{\partial x}=-\frac{\mu}{K}u-g\rho(a,b), \tag{3}$$

$$\frac{\partial p}{\partial y}=-\frac{\mu}{K}v, \tag{4}$$

$$\frac{\partial a}{\partial t}+u\frac{\partial a}{\partial x}+v\frac{\partial a}{\partial y}=D_A\left(\frac{\partial^2 a}{\partial x^2}+\frac{\partial^2 a}{\partial y^2}\right)-k_0ab^2, \tag{5}$$

$$\frac{\partial b}{\partial t}+u\frac{\partial b}{\partial x}+v\frac{\partial b}{\partial y}=D_B\left(\frac{\partial^2 b}{\partial x^2}+\frac{\partial^2 b}{\partial y^2}\right)+k_0ab^2, \tag{6}$$

where we made the standard Boussinesq approximation. The density ρ is given by an "equation of state,"

$$\rho(a,b)=\rho_0+\gamma_1 a+\gamma_2 b, \tag{7}$$

where $\rho_0=\rho(0,0)$ is the fluid density in the absence of A and B and $\gamma_{1,2}$ are the solutal expansion coefficients of species A and B. We assume that γ_1 and γ_2 are of the same sign and without any loss in generality we can take them both as positive. In the above, the pressure p is independent of the distance across the gap. The velocity components u and v (in the x and y directions, respectively) and the concentrations a and b are their values averaged across the gap, following the standard derivation of the equations for a Hele–Shaw cell. ρ is the density, g is the effective acceleration due to gravity, μ is the viscosity of the fluid, and K the permeability, which, for Hele–Shaw cells, is related to the thickness h_0 of the cell by $K=h_0^2/12$. D_A and D_B are the diffusion coefficients of reactants A and B.

Initially, ahead of the reaction front, there is only A present, at uniform concentration a_0. This is converted fully into B by reaction (1), hence the reaction product is also at the same uniform concentration a_0. We make Eqs. (2)–(7) dimensionless by introducing the time T_0, length L_0, and velocity U_0 scales, all based on reaction (1),

$$T_0=\frac{1}{k_0a_0^2},\quad L_0=\left(\frac{D_A}{k_0a_0^2}\right)^{1/2},\quad U_0=(D_Ak_0a_0^2)^{1/2}. \tag{8}$$

We then write

$$(u,v) = U_0(\bar{u},\bar{v}), \quad (x,y) = L_0(\bar{x},\bar{y}), \quad t = T_0\bar{t},$$
$$p = \frac{\mu D_A}{\rho_0 K}\bar{p}, \quad (a,b) = a_0(\bar{a},\bar{b}). \tag{9}$$

In addition, we scale the density as $\bar{\rho}=\rho/\Delta\rho$, where $\Delta\rho=(\gamma_1-\gamma_2)a_0$. This leads to the dimensionless equations for our model as, on dropping the bars for convenience,

$$\frac{\partial^2\psi}{\partial x^2}+\frac{\partial^2\psi}{\partial y^2} = -\left(R_a\frac{\partial a}{\partial y}+R_b\frac{\partial b}{\partial y}\right), \tag{10}$$

$$\frac{\partial a}{\partial t}+\frac{\partial\psi}{\partial y}\frac{\partial a}{\partial x}-\frac{\partial\psi}{\partial x}\frac{\partial a}{\partial y} = \left(\frac{\partial^2 a}{\partial x^2}+\frac{\partial^2 a}{\partial y^2}\right)-ab^2, \tag{11}$$

$$\frac{\partial b}{\partial t}+\frac{\partial\psi}{\partial y}\frac{\partial b}{\partial x}-\frac{\partial\psi}{\partial x}\frac{\partial b}{\partial y} = D\left(\frac{\partial^2 b}{\partial x^2}+\frac{\partial^2 b}{\partial y^2}\right)+ab^2, \tag{12}$$

where we introduced the stream function ψ, defined such that $u=\partial\psi/\partial y$, $v=-\partial\psi/\partial x$ and eliminated the pressure from the equations. Here

$$D = \frac{D_B}{D_A}, \tag{13}$$

$$R_a = \frac{\gamma_1 K g a_0}{\mu U_0} = \frac{\gamma_1 K g}{\mu(D_A k_0)^{1/2}}, \tag{14}$$

$$R_b = \frac{\gamma_2 K g a_0}{\mu U_0} = \frac{\gamma_2 K g}{\mu(D_A k_0)^{1/2}}. \tag{15}$$

For families of reactions like the IAA reaction, the density of the product after the passage of the wave is less than that of the initial reactants.[1,2] From this it follows that $\gamma_1>\gamma_2$ and we have, from Eqs. (14) and (15), that $R_a>R_b$. This means that upward propagating fronts will become buoyantly unstable through a RT instability. If, however, we take $\gamma_1<\gamma_2$, as in the CT reaction case for instance, the reaction products are denser than the unreacted state and $R_a<R_b$.

For a given autocatalytic reaction, γ_1 and γ_2 are fixed and the Rayleigh numbers in Eqs. (14) and (15) can be varied by changing the gap width h_0 (which alters the permeability K) or g. Modifying g can be achieved by varying the angle θ of the experimental setup with the vertical.[15] It is interesting to note, at least for the cubic autocatalytic scheme given by (1), that the Rayleigh numbers are independent of a_0. For kinetics of orders different to this, the Rayleigh numbers will also depend on the initial concentrations. The angle θ, the gap width h_0, the viscosity μ, and the initial concentration a_0 are then the quantities that can be varied experimentally so as to affect the properties of the RT instability. In parallel, to obtain a diffusive instability, we can slow down the diffusion of the autocatalytic species D_B by binding B with large molecules.[27] By changing these various parameters appropriately, the time scales of the buoyancy and diffusive instabilities can be made of the same order of magnitude, thus allowing them to interact.

III. LINEAR STABILITY ANALYSIS

We first derive the traveling waves that are the base state of our LSA before analyzing the various stability scenarios.

A. Planar traveling waves

Initially $a=1$, $b=0$, and $\psi=0$ (no flow) with a local input of B applied across the reactor to start the reaction. This leads to a pair of counter-propagating reaction-diffusion fronts, one propagating upwards and the other one downwards.[52] It is these reaction fronts that can be modified by buoyancy-driven and diffusion-driven instabilities. We start by describing the planar traveling waves that our system can support, the base state for our LSA.

To consider the planar propagating reaction fronts, we introduce the traveling coordinate $\zeta=x-ct$, where c is the constant wave speed, and look for a solution of Eqs. (11) and (12) in the form $a=a(\zeta)$, $b=b(\zeta)$. This leads to the traveling wave equations, in the absence of flow,

$$a''+ca'-ab^2=0, \quad Db''+cb'+ab^2=0, \tag{16}$$

on $-\infty<\zeta<\infty$, subject to

$$a\to 1, \quad b\to 0 \quad \text{as} \quad \zeta\to\infty, \quad a\to 0, \quad b\to 1 \quad \text{as} \quad \zeta\to-\infty, \tag{17}$$

where primes denote differentiation with respect to ζ. The solution to the traveling wave [Eqs. (16) and (17)] determines the wave speed c, which depends on the ratio of diffusion coefficients D, with c decreasing to zero as D is decreased. The solution to Eqs. (16) and (17) is discussed fully in Refs. 45 and 46.

To consider the stability of the reaction fronts to a buoyancy-driven instability, we perturb about the planar traveling wave solution given by Eqs. (16) and (17) by putting

$$a(\zeta,y,t) = a(\zeta)+A(\zeta,y,t), \quad b(\zeta,y,t) = b(\zeta)+B(\zeta,y,t), \tag{18}$$

where A, B, and $\psi=\psi(\zeta,y,t)$ are assumed small. We then look for a solution of the resulting linearized equations in the form

$$(A,B,\psi) = e^{\sigma t+iky}(A_0(\zeta),B_0(\zeta),\psi_0(\zeta)). \tag{19}$$

This leads to an eigenvalue problem for (A_0,B_0,ψ_0) in terms of the growth rate σ and the wave number k as

$$A_0''+cA_0'-(b^2+k^2+\sigma)A_0-2abB_0-a'u_0=0, \tag{20}$$

$$DB_0''+cB_0'-(Dk^2-2ab+\sigma)B_0+b^2A_0-b'u_0=0, \tag{21}$$

$$u_0''-k^2u_0-k^2(R_aA_0+R_bB_0)=0, \tag{22}$$

where $u_0=ik\psi_0$, subject to

$$A_0\to 0, \quad B_0\to 0, \quad u_0\to 0 \quad \text{as} \quad \zeta\to\pm\infty, \tag{23}$$

i.e., the perturbations must decay far away from the front.

We obtained dispersion curves, plots of σ against k for given values of R_a, R_b, and D by solving Eqs. (20)–(22) numerically by a shooting method. This required the solution to the traveling wave [Eqs. (16) and (17)] and built in the

TABLE I. Summary of the stabilizing (+) and destabilizing (−) influences of the buoyancy effects (buoy) of the differential diffusive effects (diff.) and the fact that $D>1$ ($D<1$) is making the RD base state front faster or slower than for $D=1$ (RD) in the case when $R_a>R_b$. In the stability properties, "monotonous" and "nonmonotonous" refer to the dependence of $\sigma_{\max}$ on D for each case as seen on Figs. 3(b) and 4(b), respectively.

Case	Direction	D	Buoy	Diff.	RD	Stability	Figure
1	Up	$D=1$	−	Neutral	Neutral	RT unstable	2
2	Up	$D>1$	−	−	+	Monotonous	3
3	Up	$D<1$	−	+	−	Nonmonotonous	4 and 5
4	Down	$D=1$	+	Neutral	Neutral	Always stable	
5	Down	$D>1$	+	+	+	Always stable	
6	Down	$D<1$	+	−	−	Enhanced diffusional instability if $D<D_c$	7 and 8

asymptotic forms for the solution as $\zeta\to\pm\infty$ resulting from Eq. (23). One of the arbitrary constants that appeared in this development is put to unity to force a nontrivial solution. The resulting (linear) boundary-value problem was solved using a standard shooting method (D02AGF in the Numerical Algorithms Group library[53]). This method converged easily and enabled the dispersion curves to be readily calculated. The same general approach was used to solve the traveling wave problems (16) and (17).

We need to consider how to choose the parameters R_a and R_b. We have from Eqs. (14) and (15) that

$$\frac{R_b}{R_a}=\frac{\gamma_2}{\gamma_1}=\alpha, \tag{24}$$

since for a given chemical system, we can expect the ratio γ_2/γ_1 to be a constant. Our results are based on this ratio being fixed at some given value α, i.e., we take $R_b=\alpha R_a$ throughout. We treat two separate cases. For the IAA system experimental results suggest that $\gamma_2/\gamma_1\simeq 0.5$, which leads us to take $\alpha=0.5$ or $R_b=0.5R_a$ for our first case. For our second case we consider the situation when R_a is less than R_b as in the CT system, taking $\alpha=2.0$, i.e., $R_b=2.0R_a$.

The change in density $\Delta\rho=\rho_a-\rho_b$ across the reaction front is given by, from Eq. (7),

$$\Delta\rho=(\gamma_1-\gamma_2)a_0=\frac{\mu(D_Ak_0)^{1/2}a_0}{Kg}(R_a-R_b)=(1-\alpha)\gamma_1a_0, \tag{25}$$

in our case. Keeping the ratio $\alpha=R_a/R_b$ fixed is, from Eq. (24), the same as keeping the ratio γ_1/γ_2 fixed. In our first case $\alpha<1$ and, from Eq. (25), this means that there is a decrease in density across the front (for a given initial concentration a_0 of reactant A). In this case upward propagating fronts have an inherent buoyant instability with downward propagating fronts being buoyantly stable. The converse is true for our second case.[47] Here $\alpha>1$, giving an increase in density across the front. Consequently it will now be the downward propagating fronts that have the inherent buoyant instability with upward propagating fronts being buoyantly stable. Our main aim is to see to what extent these inherent stability characteristics arising from density changes across the reaction front are altered by having differential diffusion of the reacting species. In order to do so, we analyze the two cases $\alpha<1$ and $\alpha>1$ separately.

B. Dispersion curves for $R_a>R_b$

This case is motivated by those chemical reactions for which the products of the reaction are lighter than the initial reactants, a typical example being the IAA system for which reaction scheme (1) is a good model. This system has $\gamma_2/\gamma_1<1$ and hence $R_a>R_b$. In the absence of differential diffusion between reactant A and product B (i.e., for $D=1$), the only source of an instability is that related to buoyancy effects arising whenever $R_a\neq R_b$. We start by taking $R_a>R_b$, i.e., $\alpha<1$ and $D=1$, for which upward propagating waves are the buoyantly unstable ones (case 1, Table I), the descending fronts remaining planar[48] (case 4, Table I) for $D=1$. We now examine what new physical mechanisms come into play when $D\neq 1$.

If $D>1$, i.e., if the product B diffuses faster than the reactant A, then differential diffusion has a destabilizing influence on the RT instability for ascending fronts while it stabilizes descending fronts.[41] This can be understood from the displacement particle argument shown in Fig. 1. Consider a stratification of a species A on top of B (upper part of Fig. 1). In a concave perturbation around a planar front, as shown in Fig. 1, the upper species A diffuses out of the concave part and is thus diluted. This decreases the density difference across the front and stabilizes the RT instability with regard

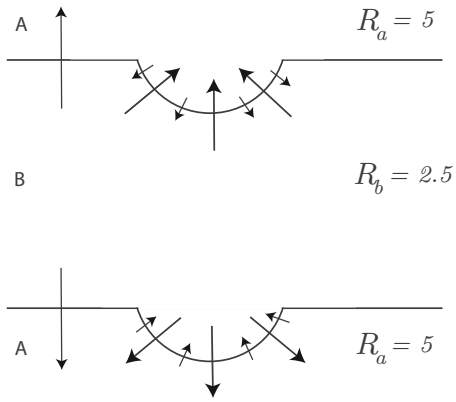

FIG. 1. Displaced particle argument for $D>1$ (i.e., $D_B>D_A$). The fact that the product B diffuses faster than reactant A has a destabilizing effect on the RT instability of ascending fronts (upper part), while it stabilizes buoyantly stable descending ones (lower part) even more. The long and short arrows in the front perturbation indicate the differential intensity of diffusion of B and A, respectively, while the arrow in the planar part indicates the direction of propagation of the front.

to the planar situation. On the contrary, the lower species B is concentrated into the concave part, which increases the density difference and enhances the RT destabilization. A reverse reasoning operates in convex perturbations. Hence enhancement of the RT instability wins for ascending fronts (for which B lies underneath A) if $D_B > D_A$, i.e., the lower species diffuses faster than the upper species. These differential diffusion effects come into play as soon as there is a local change in curvature of the front and are independent of the values of the Rayleigh numbers. Thus there is enhancement of the RT instability if $D > 1$ for ascending fronts for both $R_a > R_b$ (case 2) and $R_b > R_a$ (case 8). A similar argument shows that, for descending fronts, differential diffusion enhances the RT instability if the species on top diffuses faster than the lower one, i.e., if $D < 1$ for both $R_a > R_b$ (case 6) and $R_a < R_b$ (case 12).

This influence is, however, competing with the fact that reaction-diffusion (RD) fronts also travel faster when $D > 1$ because faster diffusion of B gives an excess of autocatalytic species ahead of the front, which is speeding it up. The fact that the front then travels faster makes it more difficult for the RT instability to develop.[37] These various trends are summarized in Table I, where we mention whether the buoyancy effects, the differential diffusivity effects, and the fact that the RD speed depends on the value of D have a stabilizing (positive sign in the table) or destabilizing (negative sign in the table) influence on the dynamics. We now consider the dispersion curves, which result from the combination of these three effects.

1. Upward propagating fronts

We start by taking $R_b = 0.5R_a$ and focus on the case where A and B diffuse at the same speed ($D=1$). Figure 2(a) shows dispersion curves for $R_a = 2.0, 5.0$ ($R_b = 1.0, 2.5$) (case 1, Table I) for this case. Both the range of unstable wave numbers and the maximum growth rate $\sigma_{\max}$ increase as R_a (and hence R_b) is increased. This is to be expected as the density difference across the front, given by Eq. (25), is then increasing. This is made clearer in Fig. 2(b) where we plot $\sigma_{\max}$ against R_a. The rate of increase in $\sigma_{\max}$ with R_a appears almost linear for the larger values of R_a. When $R_a = 0$, $\sigma_{\max} = 0$ as the system is then buoyantly marginally stable while the diffusive instability cannot set in as $D = 1$. (In this and subsequent figures, • corresponds to values of parameters used for the numerical integrations.)

For $D > 1$ (case 2, Table I and Fig. 3), both the range of unstable wave numbers and the maximum growth rates decrease for a given value of R_a, as can be seen in Fig. 3(a), comparing the dispersion curves for $D = 1.0$ and 2.0 at fixed Rayleigh numbers. In Fig. 3(b), the plot of $\sigma_{\max}$ against D, again for $R_a = 5.0$, $R_b = 2.5$, shows that $\sigma_{\max}$ decreases monotonically as D is increased from $D = 1$. There is also an associated decrease in the range of unstable wave numbers as D is increased. Thus the stabilizing effects of increased propagation speeds outweigh the destabilizing effect of differential diffusion (at least for these parameter values).

For $D < 1$ (case 3, Table I), we again have two competing effects, differential diffusion for $D < 1$ has a stabilizing influence on the RT instability (see Fig. 1), however, the RD

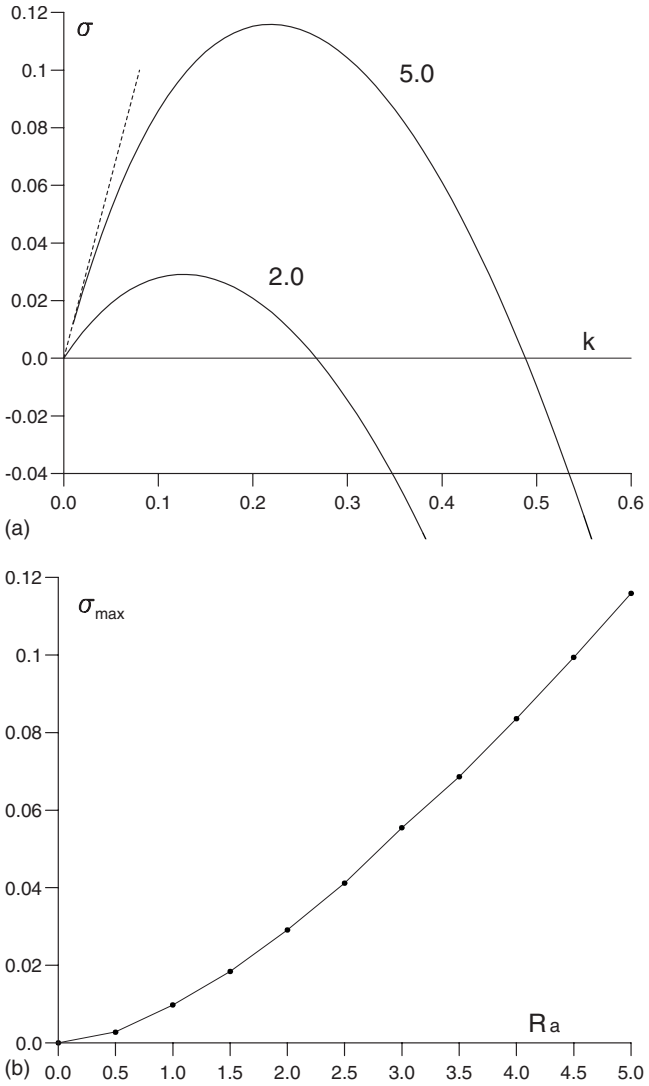

FIG. 2. Stability results for the pure RT instability of ascending fronts obtained for $D = 1.0$. (a) Dispersion curves for $R_a = 2.0, 5.0$, ($R_b = 1.0, 2.5$). Expression (41) for k small is shown by the broken line. (b) A plot of $\sigma_{\max}$, the maximum value of the growth rate σ, against R_a (with $R_b = 0.5R_a$).

fronts are also moving slower, which is favoring the destabilizing buoyancy effects. The competition between these effects leads to a nonmonotonous dependence of the dispersion curves on D (see Fig. 4). When D is reduced from $D = 1$, the range of unstable wave numbers and the maximum growth rates increase, at least initially, probably because the RD front moves slower allowing the buoyancy effects to be more operative than when $D = 1$. However, there is a value of D at which both the range of unstable wave numbers and the maximum growth rates start to decrease as D is decreased further. This is due to the fact that the stabilizing influence of differential diffusion then takes over. This is illustrated in Fig. 4(a), showing dispersion curves for varying D at fixed $R_a = 0.5$ and more clearly in Fig. 4(b), where $\sigma_{\max}$ is plotted against D. This figure suggests that $\sigma_{\max}$ achieves its greatest value at $D \simeq 0.35$ (for these values of R_a and R_b). In Fig. 4 and some other subsequent figures, we also plot as Δ growth rates obtained by following the early time linear growth of the transverse modulation of the interface as a function of

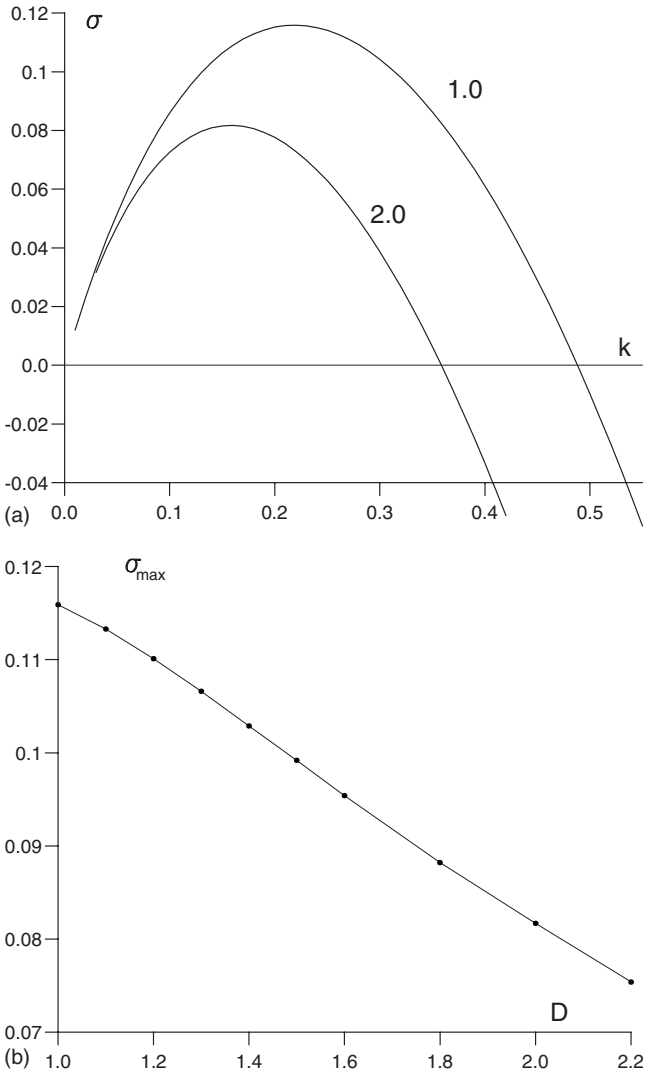

FIG. 3. Stabilizing influence of $D>1$ on the RT instability of ascending fronts for $R_a=5.0$, $R_b=2.5$. (a) Dispersion curves for $D=1.0, 2.0$. (b) A plot of σ_{max}, the maximum value of the growth rate σ, against D.

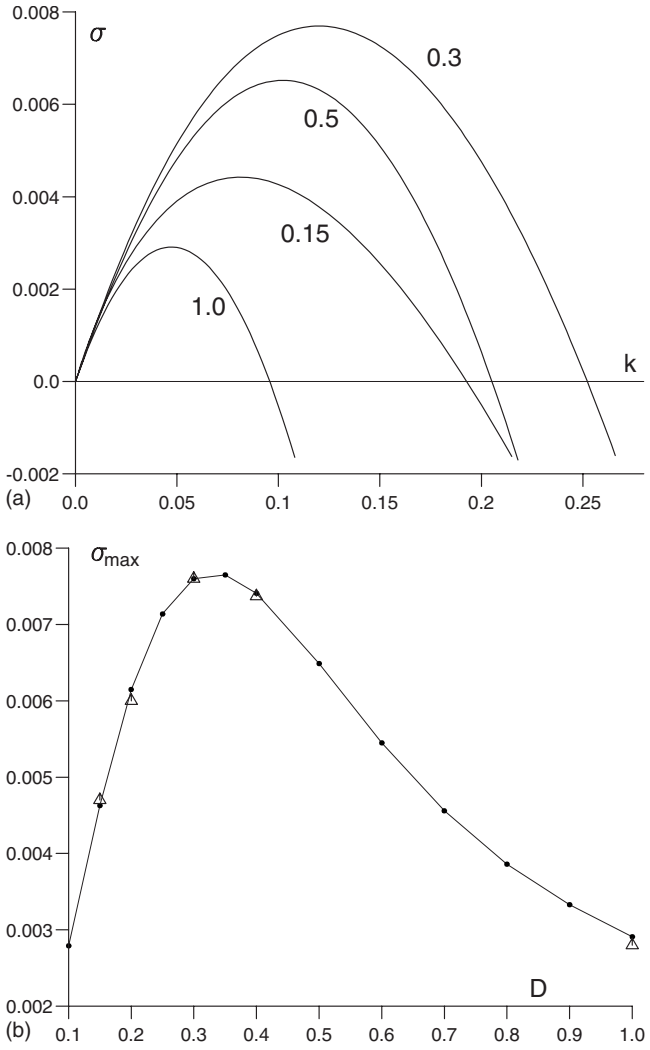

FIG. 4. Influence of $D<1$ on the RT instability of ascending fronts for $R_a=0.5$, $R_b=0.25$. (a) dispersion curves for $D=1.0, 0.5, 0.3, 0.15$. (b) A plot of σ_{max}, the maximum value of the growth rate σ, against D. The values of σ_{max} obtained directly from the growth of fingers at early times in full nonlinear simulations are shown by △.

time in the full nonlinear simulations of Eqs. (10)–(12). Good agreement between the results from the LSA and from the nonlinear simulations are obtained.[43]

At the smaller values of D, the system is also diffusionally unstable, diffusional instability requiring $D<D_c \simeq 0.424$ for the cubic kinetics [Eq. (1)]. Figure 5(a) compares dispersion curves of the purely diffusional instability case ($D=0.15$, $R_a=R_b=0$) to those obtained for parameters such that the system is both diffusionally and buoyantly unstable. For $R_a=0.5$ the growth rates are comparable with those for the $R_a=0$ case, though the range of unstable wave numbers is somewhat less. As R_a (and hence R_b) is increased the maximum growth rate increases, though the range of unstable wave numbers does not appear to change significantly. In Fig. 5(b) σ_{max} is plotted against R_a for $D=0.15$, which shows that σ_{max} has a minimum value at $R_a \simeq 0.2$ before increasing with R_a. For larger values of R_a, σ_{max} increases rapidly, soon becoming much larger than the diffusional instability value of $\sigma_{max}=0.004\,34$ obtained for $R_a=0$. Also plotted in Fig. 5(b) are the values of σ_{max} for $D=1.0$ for smaller values of R_a [highlighting the small R_a part of Fig. 2(b)] to compare with the values for $D=0.15$. For small values of R_a the system is more unstable with $D=0.15$, arising mainly from the fact that the system is also diffusionally unstable for this value of D ($\sigma_{max}>0$ at $R_a=0$), whereas with $D=1.0$, it is stable at $R_a=0$ ($\sigma_{max}=0$ at $R_a=0$). However, the system with $D=1.0$ becomes the more unstable one (greater values of σ_{max}) at $R_a \simeq 0.9$.

To understand the nonmonotonous character of the dependence of σ on R_a when $D<D_c$, we refer to the displaced particle argument of Fig. 6. The unstable diffusive character of the front when $R_a=0$ is usually understood as follows:[27] in the concave part of the perturbation as seen on Fig. 6 (upper part), A is diluted out of the perturbation. There is thus less reactant A ahead of the front, which slows down its progression favoring the growth in amplitude of the perturbation and destabilizing the front. On the contrary, the autocatalyst B gets concentrated ahead of the perturbation speeding up the front that tends to go back to its planar form, thus stabilizing the system. A diffusive instability is observed when the destabilizing diffusion of A wins over the stabilizing diffusion

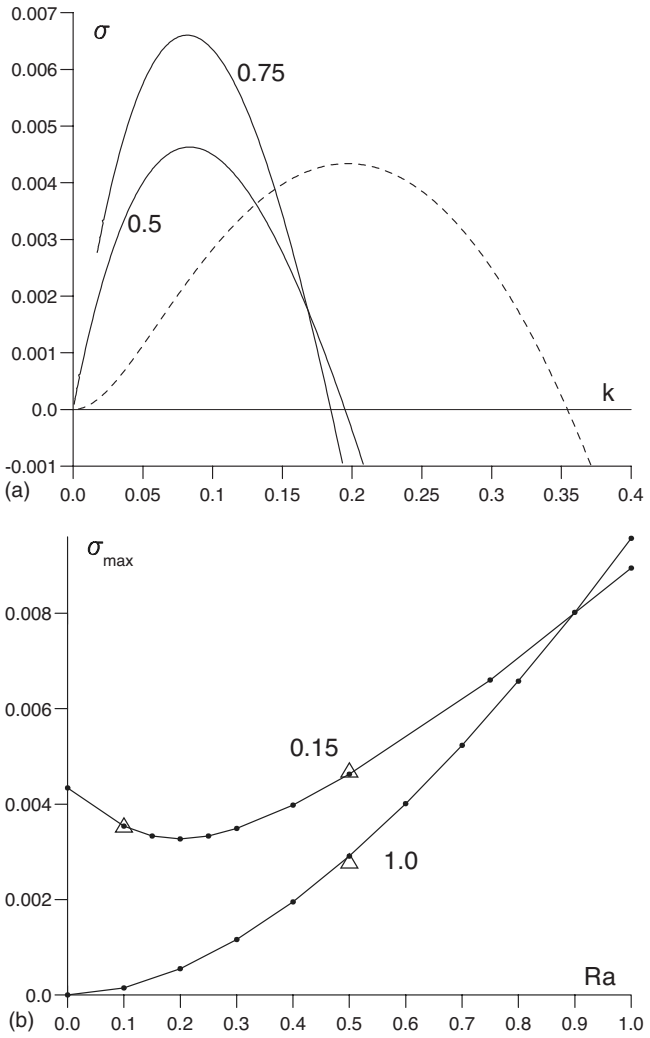

FIG. 5. Stability results for the diffusionally unstable case for ascending fronts. (a) Dispersion curves for $D=0.15$, $R_a=0.5,0.75$ (with $R_b=0.5R_a$). The pure diffusionally instability dispersion curve is shown by the broken curve ($D=0.15$, $R_a=0$). (b) $\sigma_{\max}$, the maximum value of the growth rate σ, plotted against R_a for $D=1.0$ and 0.15. The values of $\sigma_{\max}$ obtained from nonlinear simulations are shown by △.

of B, i.e., when $D_A > D_B$ and in practice when $D < D_c$. However, if $R_a > R_b$, A is denser than B, which then counteracts the diffusive growth of the perturbation. This stabilizing buoyancy effect decreases the growth rate of the diffusive instability for moderate values of R_a. However, when R_a is further increased, the standard RT instability takes over and the growth rate again becomes an increasing function of R_a [see Fig. 5(b)]. The transition from density effects stabilizing the diffusive instability at moderate values of R_a and destabilizing buoyancy effects at larger R_a lead to the nonmonotonous character of the curve for $D=0.15$ seen in Fig. 5(b).

A comparison with a similar curve for $D=1$ in Fig. 5(b), for which there are no diffusive instabilities, shows, as expected, that the larger values of $\sigma_{\max}$ for small R_a and $D<1$ are clearly related to the differential diffusivity of A and B. For $R_a \gtrsim 0.9$, the system is more unstable for $D=1$ than for $D=0.15$ as $D<1$ has a stabilizing effect on the RT instability as explained in Fig. 1. Below $R_a \simeq 0.2$, the diffusive instability takes over so that the curve of $\sigma_{\max}$ against R_a increases until the pure diffusive instability threshold is reached at $R_a=0$.

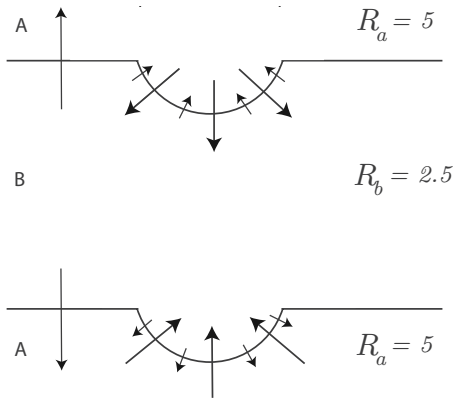

FIG. 6. Displaced particle argument for $D<1$ showing how the fact that $R_a > R_b$ stabilizes the differential diffusive instability at least for small Rayleigh numbers as seen on Fig. 5.

The dispersion curves shown in Figs. 2(a), 3(a), and 4(a) have a similar form for small values of k. This leads us to obtain a solution of the LSA [Eqs. (20)–(22)] valid for small k.

2. Solution for small k

To obtain a solution of Eqs. (20)–(22) valid for small k, we expand

$$A_0 = \tilde{A}_0 + k\tilde{A}_1 + k^2\tilde{A}_2 + \cdots,$$

$$B_0 = \tilde{B}_0 + k\tilde{B}_1 + k^2\tilde{B}_2 + \cdots, \tag{26}$$

$$u_0 = kU_1 + k^2U_2 + \cdots, \quad \sigma = k\sigma_0 + k^2\sigma_1 + \cdots.$$

The equations for $\tilde{A}_0$ and $\tilde{B}_0$ have the solution $(\tilde{A}_0,\tilde{B}_0) = (a',b')$, where (a,b) is the traveling wave solution given by Eqs. (16) and (17).

At $O(k)$ we have $U_1''=0$ and we take U_1 to be a, as yet undetermined, constant. The equations for $(\tilde{A}_1,\tilde{B}_1)$ are then

$$\tilde{A}_1'' + c\tilde{A}_1' - b^2\tilde{A}_1 - 2ab\tilde{B}_1 = (\sigma_0 + U_1)a', \tag{27}$$

$$D\tilde{B}_1'' + c\tilde{B}_1' + b^2\tilde{A}_1 + 2ab\tilde{B}_1 = (\sigma_0 + U_1)b'. \tag{28}$$

Now Eqs. (27) and (28) have a complementary function (a',b'), which satisfies the (homogeneous) boundary conditions given in Eq. (23). Thus, any solution to Eqs. (27) and (28), which satisfies homogeneous boundary conditions, must also satisfy a compatibility condition. To determine this condition we follow[35] and construct the adjoint problem $(U(\zeta),V(\zeta))$ for Eqs. (27) and (28), namely,

$$\frac{d}{d\zeta}(e^{c\zeta}U') - b^2(e^{c\zeta}U - e^{c\zeta/D}V) = 0,$$

$$\frac{d}{d\zeta}(De^{c\zeta/D}V') - 2ab(e^{c\zeta}U - e^{c\zeta/D}V) = 0, \tag{29}$$

subject to

$$U,V \to 0 \quad \text{as} \quad \zeta \to \pm\infty. \tag{30}$$

A full derivation of this adjoint problem is given in Ref. 35. The compatibility condition is then, again from Ref. 35,

$$(\sigma_0 + U_1)(I_1 + I_2) = 0, \tag{31}$$

where

$$I_1 = \int_{-\infty}^{\infty} e^{c\zeta} a' U d\zeta, \quad I_2 = \int_{-\infty}^{\infty} e^{c\zeta/D} b' V d\zeta.$$

It was seen in Ref. 35 that $I_1+I_2 \neq 0$ except when $D=1$, which is a degenerate case for the present analysis. Expression (31) then gives

$$\sigma_0 + U_1 = 0, \quad \text{and hence} \quad (\tilde{A}_1, \tilde{B}_1) = K_1(a', b') \tag{32}$$

for some constant K_1.

At $O(k^2)$ we then have

$$U_2'' = R_a a' + R_b b', \tag{33}$$

$$\tilde{A}_2'' + c\tilde{A}_2' - b^2\tilde{A}_2 - 2ab\tilde{B}_2 = (\sigma_0 K_1 + 1 + \sigma_1)a' + a' U_2, \tag{34}$$

$$D\tilde{B}_2'' + c\tilde{B}_2' + b^2\tilde{A}_2 + 2ab\tilde{B}_2 = (\sigma_0 K_1 + D + \sigma_1)b' + b' U_2. \tag{35}$$

Equation (33) gives

$$U_2' = R_a a + R_b b + L_2 \tag{36}$$

for some constant L_2. Clearly this does not satisfy the boundary conditions as $\zeta \to \pm\infty$ for any choice of L_2. This means that outer regions are required in which these conditions are attained. We construct two outer regions, both with independent variable $Y=k\zeta$, one in $Y>0$ and the other in $Y<0$. In these regions $A_0 \equiv 0$ and $B_0 \equiv 0$ (at least to the order we are working) and in which we put $u_0=kw$, where w satisfies

$$w'' - w = 0 \quad \text{in} \quad 0 < Y < \infty \quad \text{and in} \quad -\infty < Y < 0, \tag{37}$$

subject to the matching conditions, from Eq. (36), that

$$w \sim U_1 + (R_a + L_2)Y + \cdots \text{as} \quad Y \to 0^+,$$
$$w \sim U_1 + (R_b + L_2)Y + \cdots \quad \text{as} \quad Y \to 0^-. \tag{38}$$

The solutions to Eq. (37), which satisfies Eq. (38), are

$$w = U_1 e^{-Y} \quad \text{in} \quad Y > 0, \quad w = U_1 e^{Y} \quad \text{in} \quad Y < 0. \tag{39}$$

Applying the matching conditions (38), at $O(Y)$, in (39) gives

$$R_a + L_2 = -U_1, \quad R_b + L_2 = U_1. \tag{40}$$

From Eqs. (32) and (40) it follows that $\sigma_0=(R_a-R_b)/2$ and hence

$$\sigma \sim \frac{(R_a - R_b)}{2} k + \cdots \quad \text{for} \quad k \quad \text{small}, \tag{41}$$

independent of D, as is seen in Figs. 3(a) and 4(a). Expression (41) shows that upward propagating fronts are always buoyantly unstable, at least for sufficiently small wave numbers.

The problem for $D=1$ is somewhat simpler to deal with as the order of the system can be reduced since now $a+b \equiv 1$, $A_0+B_0 \equiv 0$. An expansion analogous to that described above can be carried out, the end result still being Eq. (41). Expression (41) for k small is plotted in Fig. 2(a) (shown by a broken line) for the $R_a=5.0$, $R_b=2.5$ case, and shows good agreement, at least for small k, with the numerically determined values of σ.

Result (41) holds for upward propagating fronts. To consider downward propagating fronts, we need only change the sign of the terms on the right-hand side of Eq. (10), corresponding to a change in sign of the buoyancy force term in Eq. (3). Consequently for the LSA, there is a change in sign for the final terms in Eq. (22). The result is that

$$\sigma \sim -\frac{(R_a - R_b)}{2} k + \cdots \quad \text{for} \quad k \quad \text{small}, \tag{42}$$

showing that σ is negative for small wave numbers for downward propagating fronts, a situation which we now consider in more detail.

3. Downward propagating fronts

Relation (41) between σ and k for k small indicates that upward propagating fronts will always be unstable for $R_a > R_b$ (cases 1–3, Table I), at least for sufficiently small wave numbers. For downward propagating fronts, the values of σ given by Eq. (42) will be negative for small wave number k. This is readily understood for $D=1$ for which the system is buoyantly stable featuring a stable density stratification of lighter products B over heavier reactant A (case 4, Table I). For $D>1$ and $R_a>R_b$ (case 5, Table I), the stabilizing effect of differential diffusion and the fact that the base state reaction front travels faster for $D>1$ (which is unfavorable to the development of the RT instability) both make descending fronts even more stable than for $D=1$.

However, when $D<1$, differential diffusion and the slower RD speed both act to destabilize the favorable density stratification (case 6, Table I) and for $D<D_c$, the system is also diffusionally unstable. It may then be possible to destabilize the system and thus have $\sigma>0$ over a finite range of nonzero wave numbers. This possibility can be seen in Fig. 7(a), where we give dispersion curves for $R_a=0.25, 0.5$ (with $D=0.15$ and $\alpha=0.5$) for downward propagating fronts. For both values of R_a, there is a finite range of wave numbers over which $\sigma>0$ and the system is unstable, even though $\sigma<0$ for small k. Note that the maximum growth rates in this case are somewhat greater than those for the upward propagating reaction fronts [compare the value of $\sigma_{\max}$ for $R_a=0.5$ in Fig. 7(a) with that in Fig. 5(a)] and are also greater than for the pure diffusional instability case ($R_a=0$), shown in Fig. 5(a) by a broken line. The system becomes more unstable with increased values for $\sigma_{\max}$ and a greater range of unstable wave numbers as R_a is increased (at least for the values of R_a tried). This can be seen in Fig. 7(b), where we plot $\sigma_{\max}$ against R_a for $D=0.15$. This figure shows

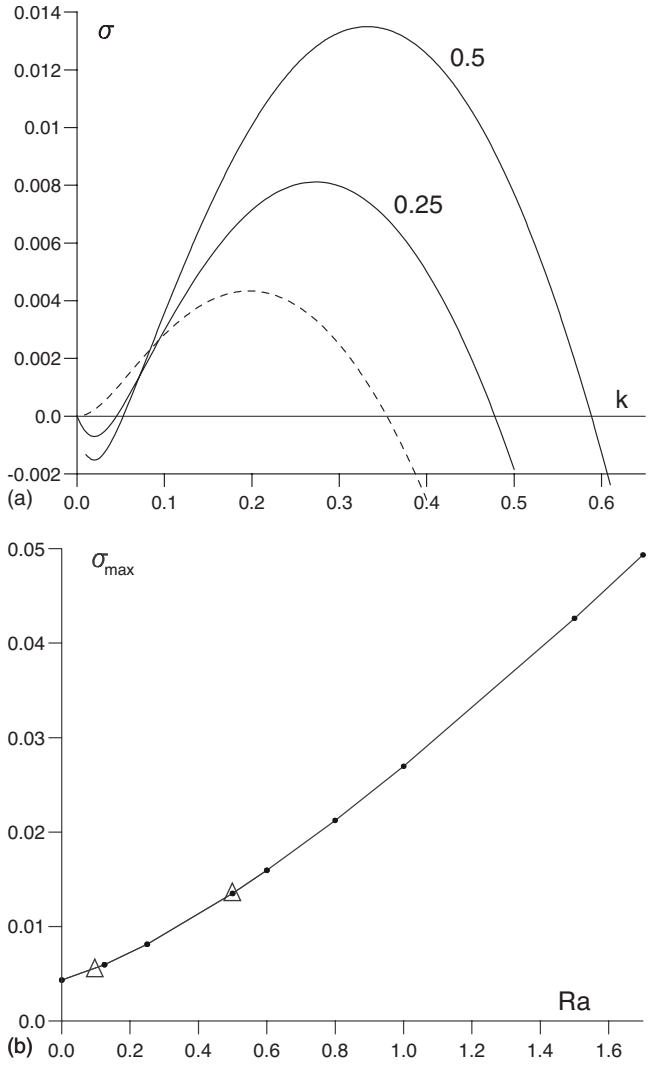

FIG. 7. Stability results for the diffusionally unstable case for descending fronts. (a) Dispersion curves for $D=0.15$, $R_a=0.25,0.5$ (with $R_b=0.5R_a$). The pure diffusionally instability dispersion curve is shown by the broken curve ($D=0.15$, $R_a=0$). (b) σ_{max}, the maximum value of the growth rate σ, plotted against R_a. The values of σ_{max} obtained directly from nonlinear simulations are shown by △.

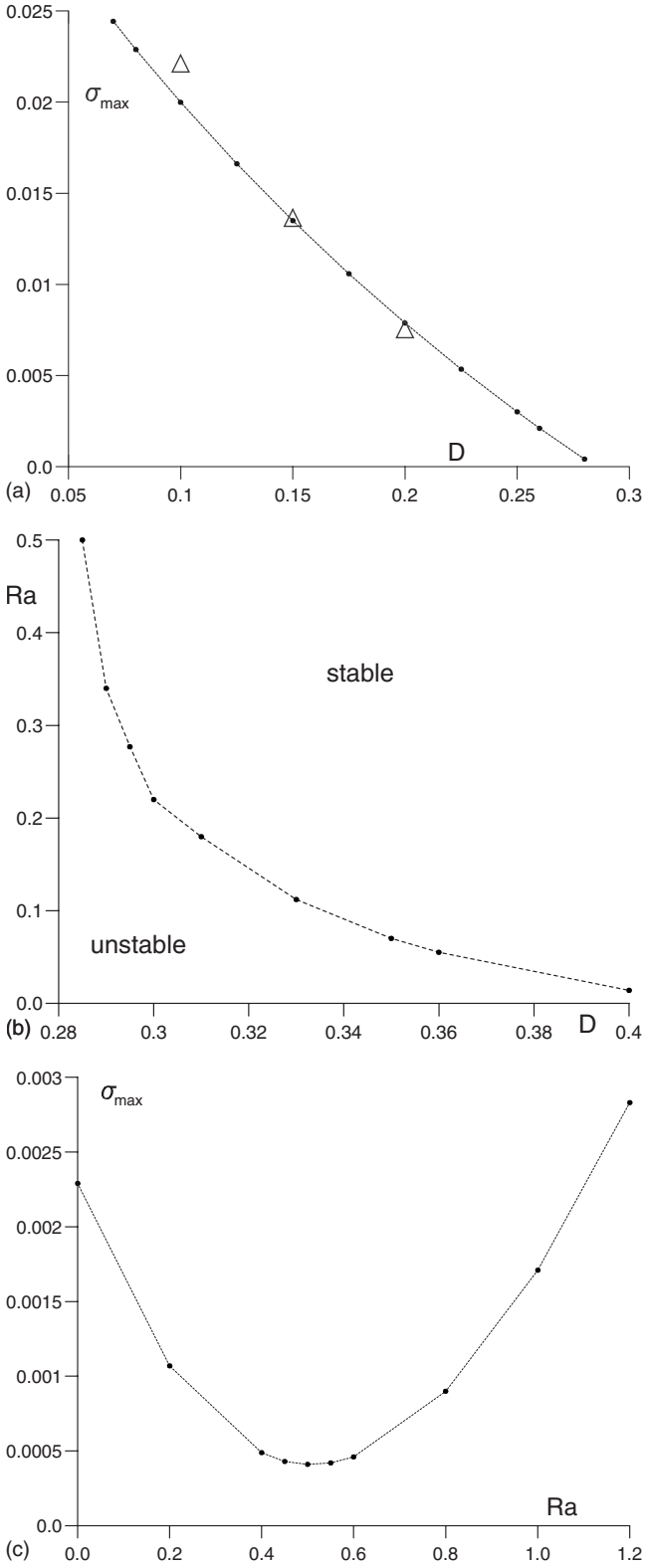

FIG. 8. Influence of $D<1$ on the RT instability of descending fronts for $R_a=0.5$, $R_b=0.25$. (a) σ_{max} plotted against D. The values of σ_{max} obtained directly from nonlinear simulations are shown by △. (b) The values of R_a at which the system changes from being unstable to being stable plotted against D. (c) σ_{max}, plotted against R_a (with $R_b=0.5R_a$) for $D=0.28<D_1$, illustrating that the system remains unstable for all R_a when $D<D_1$.

that σ_{max} is somewhat greater in this case than for the upward propagating fronts [compare with Fig. 5(b)].

The result that downward propagating fronts, which are buoyantly stable, can become more unstable than their buoyantly unstable ascending equivalent when they are diffusionally unstable is perhaps unexpected. The reason for this instability can be explained by the displaced particle argument described above and in Fig. 1 and results from the fact that having $D<1$ gives a destabilizing influence on buoyancy effects for descending fronts when $R_a>R_b$.[41] A related effect, seen when the buoyancy forces result from both concentration and temperature gradients, has already been shown to be able to destabilize a stratification of solute-light and hot products on top of solute-heavy and cold reactants in exothermic fronts.[40]

We examined this enhanced instability of downward propagating fronts in a little more detail. In Fig. 8(a) we plot σ_{max} against D for $R_a=0.5$ and descending fronts. The figure shows that σ_{max} increases as D is decreased. σ_{max} becomes zero at $D\simeq 0.285$, with the system then being fully stable at larger D for this value of R_a, i.e., has $\sigma<0$ for all $k>0$. This latter point raises the question as to how the change in stability depends on the value of R_a. In Fig. 8(b) we plot the

TABLE II. Same as Table I in the case when $R_a < R_b$.

Case	Direction	D	Buoy	Diff.	RD	Stability	Figure
7	Up	$D=1$	+	Neutral	Neutral	Stable	
8	Up	$D>1$	+	−	+	Stable	
9	Up	$D_c<D<1$	+	+	−	Stable	
9b	Up	$D<D_c$	+	−	−	Lowered diffusional instability if $D<D_c$	10
10	Down	$D=1$	−	Neutral	Neutral	RT unstable	9
11	Down	$D>1$	−	+	+	Unstable	11
12	Down	$D<1$	−	−	−	ST chaos	12 and 13

values of R_a at which the system changes from being unstable to being fully stable against D, still with $R_b=0.5R_a$. This figure shows that the region of instability (as labeled on the figure) decreases as D is increased and strongly suggests that having $D<D_c$, i.e., having the system diffusionally unstable, is a necessary requirement for downward propagating fronts to become unstable through buoyancy effects when the products are lighter than the reactants ($R_b<R_a$).

Figure 8(b) also shows that there is a value D_1 of D, with $D_1 \simeq 0.284$ such that, for $D<D_1$, the system is always unstable for all values of R_a. Thus stability can be restored by making R_a sufficiently large (i.e., increasing the stabilizing effect of having light B over heavy A) only for D in the range $D_1<D<D_c$. To illustrate this point further, $\sigma_{\max}$ is plotted against R_a in Fig. 8(c) for $D=0.28$, a value just below D_1. This figure shows that $\sigma_{\max}>0$ for all R_a, having a minimum value of $\sigma_{\max} \simeq 5\times10^{-4}$ before increasing for larger values of R_a. For values of $D>D_1$, we find that $\sigma_{\max}$ decreases to zero for increasing R_a at the values shown in Fig. 8(b) and remains zero thereafter.

C. Dispersion curves for $R_b > R_a$

We now consider those families of reactions where the products are heavier than the reactant, as in the CT system for example. For this situation we take $\alpha=2.0$, i.e., $R_b=2R_a$.

1. Upward propagating fronts

In this case, when $D=1$, it is the downward propagating fronts that are buoyantly unstable (case 10, Table II), with the upward propagating fronts being buoyantly stable (case 7, Table II), as can also be expected from Eqs. (41) and (42). In all the cases tried for $D=1$, the LSA does indeed show that upward propagating fronts are stable and that downward propagating fronts are unstable. We illustrate this by the dispersion curves for $D=1.0$ and $R_a=1.0, 2.5, 5.0$ shown in Fig. 9. A point to note from this figure is that, for a given value of R_a, the growth rates are somewhat higher than in the previous case where $R_b=0.5R_a$ [Fig. 2(a)]. This might be expected as, from Eq. (25), the same value of R_a corresponds to a greater change in density across the front in the present case, where $\alpha=2$ than in the one depicted in Fig. 2(a), where $\alpha=0.5$. If we consider values of R_a and α, which give the same density change across the front, for example, $R_a=1.0$, $\alpha=2$ in Fig. 9 with $R_a=2.0$, but $\alpha=0.5$ in Fig. 2(a), then we see comparable growth rates, as might be expected.

We now examine what happens to ascending fronts when $D \neq 1$. A displaced particle argument similar to the one given in Fig. 1 suggests that upward propagating fronts will be even more stable (i.e., have growth rates even more negative) for $D<1$ as differential diffusion is now a stabilizing mechanism (case 9, Table II). However, when $D<D_c$, the diffusional instability becomes operative, at least for small values of R_a and R_b (small density changes across the front). Hence we might expect that the dispersion curves for upward propagating fronts will have, at least for small R_a (where the buoyantly stabilizing influence of light A over heavy B is not too important), a range of unstable wave numbers where $\sigma>0$, though they will start with $\sigma<0$ from expression (41). We illustrate this possibility in Fig. 10 where we give dispersion curves for upward propagating fronts with $D=0.15$. For $R_a=0.05$ ($R_b=0.1$) the LSA suggests that the front is stable. However, for $R_a=0.025$ ($R_b=0.05$) there is a range of wave numbers for which $\sigma>0$, indicating that the front is unstable. The transition from stability to instability is at $R_a \simeq 0.0365$. If we compare, for example, the maximum growth rate $\sigma_{\max}$ for $R_a=0.025$ with that for the purely diffusional instability [Fig. 5(b)], we see that it is somewhat smaller, by a factor of approximately 0.3. This emphasizes the fact that the stabilizing effect of the buoyancy forces has here a much stronger influence than the destabilization due to differential

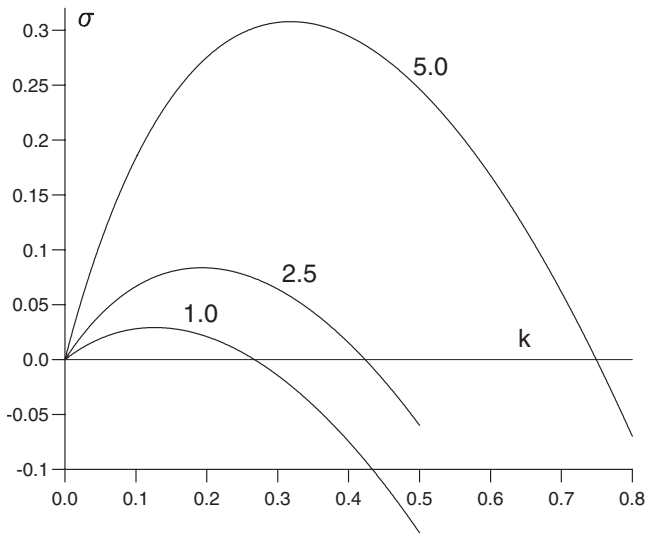

FIG. 9. Dispersion curves for $D=1.0$ and descending fronts for the case $R_b>R_a$ ($R_b=2R_a$ with $R_a=1.0, 2.5, 5.0$).

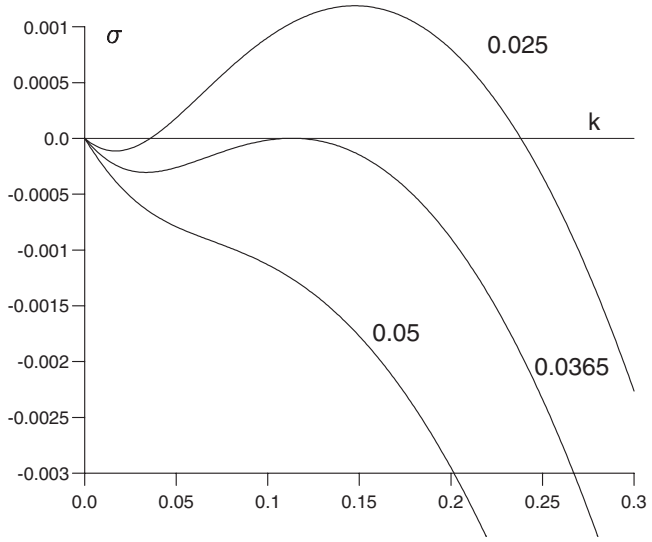

FIG. 10. Dispersion curves for $D=0.15$ (diffusionally unstable case) and $R_a=0.025$, 0.0365, 0.05 (with $R_b=2R_a$) for ascending fronts.

diffusion. This is in sharp contrast with the previous $R_a > R_b$ case for buoyantly stable descending fronts (case 6, Table I) illustrated in Figs. 7 and 8.

2. Downward propagating fronts

We now consider descending fronts for $R_b > R_a$ and $D \neq 1$. In this case, the front is RT unstable as heavy products are lying on top of lighter reactants. If $D > 1$ (case 11, Table II), differential diffusion has a stabilizing influence on the RT instability. Both $\sigma_{\max}$ and the range of unstable wave numbers decrease as D is increased from $D=1.0$, as is illustrated in Fig. 11.

The most unstable case is the one for which all three effects (buoyancy, differential diffusion and influence of $D \neq 1$ on the RD speed) are destabilizing (case 12, Table II) and this most unstable configuration occurs for descending fronts when $R_b > R_a$ and $D < 1$. This is confirmed in Fig. 12(a) featuring dispersion curves for descending, buoyantly

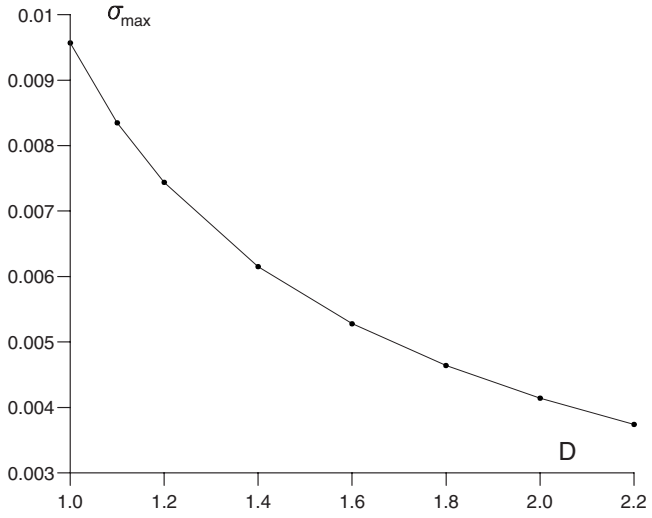

FIG. 11. $\sigma_{\max}$, the maximum value of the growth rate σ, plotted against D for $D \geq 1$ and for downward propagating fronts and the case $R_b > R_a$ with $R_a=0.5$, $R_b=1.0$.

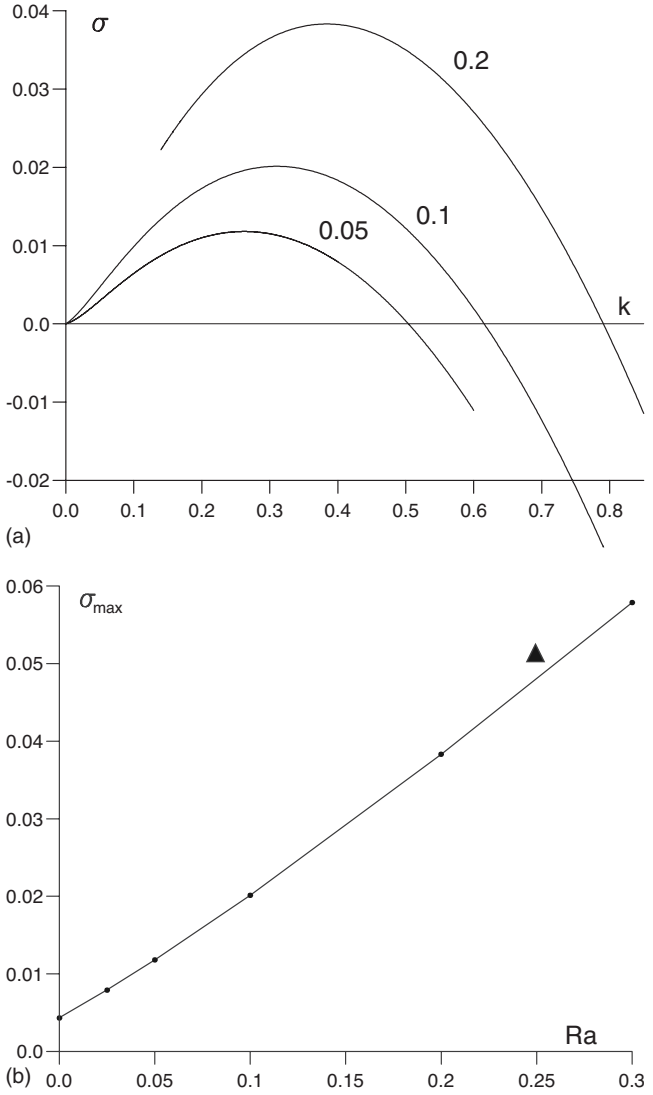

FIG. 12. Stability results for descending fronts when the system is both diffusionally and buoyantly unstable. (a) dispersion curves for $D=0.15$ and $R_a=0.05, 0.1, 0.2$ (with $R_b=2R_a$). (b) $\sigma_{\max}$, the maximum value of the growth rate σ, plotted against R_a. The values of $\sigma_{\max}$ obtained directly from the nonlinear simulations are shown by ▲.

and diffusively unstable fronts for $D=0.15$ and $R_a=0.05, 0.1, 0.2$. Values of $\sigma_{\max}$ as a function of R_a are plotted in Fig. 12(b), showing a rapid (apparently linear) increase in $\sigma_{\max}$ as R_a is increased. In this particular case, we found it more difficult to compute the dispersion curves than previously (in all other cases the calculations proceeded very easily). Even when taking very small increments in the wave number, we were unable to get the numerical scheme to converge, especially for small values of k. This might be explained by the much larger values of σ found in this case than for the $R_a > R_b$ case. For $R_a=0.2$ ($R_b=0.4$), Fig. 12(a), we find $\sigma_{\max} \simeq 0.0383$ compared to a value of $\sigma_{\max} \simeq 0.0033$ [Fig. 5(b)]. Even allowing for the different changes in density, $\sigma_{\max} \simeq 0.0040$ for $R_a=0.4$ in Fig. 5(b). In general, the values of $\sigma_{\max}$ appear to be at least an order of magnitude greater for this case. Further to this point, the range of unstable wave numbers is considerably greater for this case (compare Fig. 12(a) with Fig. 5(a) or Fig. 7(a)).

The strong destabilizing effect of the differential diffu-

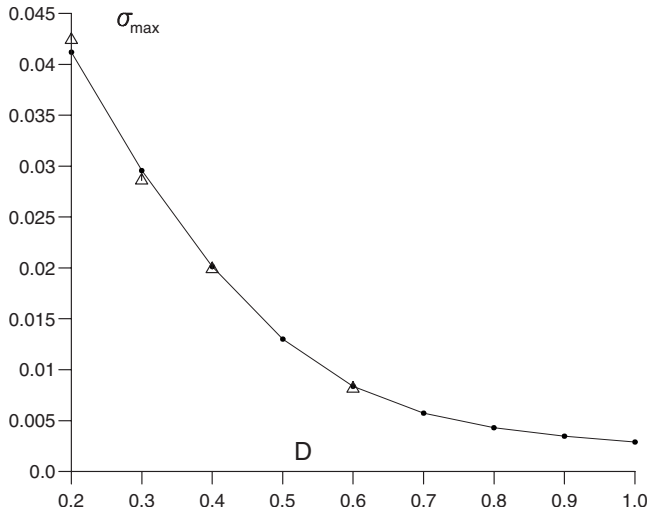

FIG. 13. σ_{max}, the maximum value of the growth rate σ, plotted against D for $D \leq 1$, downward propagating fronts in the case $R_b > R_a$ with $R_a = 0.25$, $R_b = 0.5$. The values of σ_{max} obtained directly from the nonlinear simulations are shown by $\triangle$.

sion instability on downward propagating fronts when $R_a < R_b$ can clearly be seen in Fig. 13, where we plot σ_{max} against D for $R_a = 0.25$, $R_b = 0.5$ ($\alpha = 2.0$). This figure shows a sharp increase in σ_{max} around the point where $D = D_c$. The range of unstable wave numbers is also greatly increased from $0 < k < 0.096$ for $D = 1.0$ to $0 < k < 0.731$ for $D = 0.2$.

IV. CONCLUSIONS

In autocatalytic reaction fronts where there is more than one key chemical species, it is common for the reactant A and autocatalytic product B of the reaction to have different diffusion coefficients (i.e., $D = D_B/D_A \neq 1$) and also to have different densities. Here we examined by a LSA the mutual influence of such differential diffusion and RT fingering instabilities of chemical fronts due to an unfavorable density stratification in a gravity field. We have shown that the problem can be classified into 12 different cases (Tables I and II) depending whether the front is ascending or descending in the gravity field, whether the Rayleigh number R_a of the reactant is smaller or larger than the Rayleigh number R_b of the products, and whether $D = 1$, $D < 1$, or $D > 1$. If the reactant diffuses sufficiently faster than the product ($D < D_c$), the system can also be unstable through a diffusive instability giving rise to a cellular deformation of the front.

The stability properties can be understood as the result of three effects: (i) fronts are buoyantly unstable when heavier solution lies on top of a lighter one in the gravity field, (ii) $D > 1$ ($D < 1$) is having a destabilizing (stabilizing) effect on buoyantly unstable ascending fronts while destabilizing (stabilizing) the descending fronts when $R_a > R_b$ (the reverse is true when $R_a < R_b$), and (iii) fronts travel faster for increasing values of D, which is unfavorable to the RT instability. As a corollary, slower fronts obtained when D is decreased below one are more prone to favor the RT instability. As a consequence of the competition or cooperation between these three effects, various stability scenarios have been highlighted from the LSA (giving dispersion curves i.e., the growth rate of the perturbation σ as a function of their wave number k, for various values of the parameters), as well as from analytical results for small k. This allowed to understand what kind of stability properties are to be expected if a pair of counter-propagating fronts are generated in the middle of a Hele–Shaw cell when differential diffusion phenomena are present in addition to possible buoyancy-driven instabilities.

When the reactants are heavier than the products, as in the IAA reaction for example, then, for $D = 1$, only the ascending front is buoyantly unstable and no diffusive instability can take place. If $D > 1$, the RT instability of the ascending fronts will be less efficient as $D > 1$ has a stabilizing influence, the descending front remaining stable. The most striking effect of differential diffusion comes however when $D < 1$. In this case, for ascending fronts, the most unstable growth rate σ_{max} varies nonmonotonically with D when D is decreased below one while descending fronts have their diffusive instability magnified when $D < D_c$. Buoyancy effects in this case enhance the cellular deformation due to a diffusive instability.

When the products are heavier than the reactants, as in the CT reaction, the stability scenarios are quite different. For $D = 1$, the ascending front is now buoyantly stable while the descending one features a hydrodynamic RT fingering instability. If $D > 1$, differential diffusion cannot destabilize an ascending front but can reduce the strength of the RT instability of descending fronts. When $D < D_c$, the diffusive instability of ascending fronts is lowered by buoyancy effects. The most interesting situation occurs on descending fronts when $D < D_c < 1$, in which case all effects combine to strongly destabilize the front.

The classification given in this article should allow us to predict all possible stability conditions of autocatalytic fronts where the density either decreases or increases across the front and the two key species diffuse at different rates. In order to give insight into the spatiotemporal dynamics that might be observed experimentally in the various stability scenarios studied here, numerical simulations of the full nonlinear problem have been performed and are detailed in a companion paper.[43]

ACKNOWLEDGMENTS

A.D. thanks A. Tóth and D. Horváth for fruitful discussions and acknowledges financial support from FNRS, Prodex and the Communauté franaise de Belgique (ARC program). J.D. benefitted from a FRIA Ph.D. fellowship.

[1] J. A. Pojman, I. R. Epstein, T. J. McManus, and K. Showalter, J. Phys. Chem. **95**, 1299 (1991).
[2] J. Masere, D. A. Vasquez, B. F. Edwards, J. W. Wilder, and K. Showalter, J. Phys. Chem. **98**, 6505 (1994).
[3] M. R. Carey, S. W. Morris, and P. Kolodner, Phys. Rev. E **53**, 6012 (1996).
[4] M. Böckmann and S. C. Müller, Phys. Rev. Lett. **85**, 2506 (2000).
[5] J. Martin, N. Rakotomalala, D. Salin, and M. Böckmann, Phys. Rev. E **65**, 051605 (2002).
[6] M. Böckmann and S. C. Müller, Phys. Rev. E **70**, 046302 (2004).
[7] M. C. Rogers and S. W. Morris, Phys. Rev. Lett. **95**, 024505 (2005).
[8] L. Sebestikova, J. D'Hernoncourt, M. J. B. Hauser, S. C. Müller, and A. De Wit, Phys. Rev. E **75**, 026309 (2007).

[9] I. P. Nagy, A. Keresztessy, J. A. Pojman, G. Bazsa, and Z. Noszticzius, J. Phys. Chem. **98**, 6030 (1994).
[10] A. Keresztessy, I. P. Nagy, G. Bazsa, and J. A. Pojman, J. Phys. Chem. **99**, 5379 (1995).
[11] J. A. Pojman, A. Komlósi, and I. P. Nagy, J. Phys. Chem. **100**, 16209 (1996).
[12] M. Matalon and B. J. Matkowsky, Combust. Sci. Technol. **34**, 295 (1983).
[13] N. Vladimirova and R. Rosner, Phys. Rev. E **67**, 066305 (2003).
[14] J. D'Hernoncourt, A. Zebib, and A. De Wit, Chaos **17**, 013109 (2007).
[15] D. Horváth, T. Bánsági, Jr., and A. Tóth, J. Chem. Phys. **117**, 4399 (2002).
[16] T. Bánsági, Jr., D. Horváth, Á. Tóth, J. Yang, S. Kalliadasis, and A. De Wit, Phys. Rev. E **68**, 055301 (2003).
[17] T. Bánsági, Jr., D. Horváth, and Á. Tóth, Phys. Rev. E **68**, 026303 (2003).
[18] T. Bánsági, Jr., D. Horváth, and Á. Tóth, Chem. Phys. Lett. **384**, 153 (2004).
[19] T. Bánsági, Jr., D. Horváth, and Á. Tóth, J. Chem. Phys. **121**, 11912 (2004).
[20] T. Rica, D. Horváth, and Á. Tóth, Chem. Phys. Lett. **408**, 422 (2005).
[21] D. Horváth, S. Tóth, and Á. Tóth, Phys. Rev. Lett. **97**, 194501 (2006).
[22] T. Tóth, D. Horváth, and Á. Tóth, Chem. Phys. Lett. **442**, 289 (2007).
[23] T. Tóth, D. Horváth, and Á. Tóth, J. Chem. Phys. **127**, 234506 (2007).
[24] G. Bazsa and I. R. Epstein, J. Phys. Chem. **89**, 3050 (1985).
[25] I. Nagypál, G. Bazsa, and I. R. Epstein, J. Am. Chem. Soc. **108**, 3635 (1986).
[26] J. A. Pojman, I. P. Nagy, and I. R. Epstein, J. Phys. Chem. **95**, 1306 (1991).
[27] D. Horváth, V. Petrov, S. K. Scott, and K. Showalter, J. Chem. Phys. **98**, 6332 (1993).
[28] A. Malevanets, A. Careta, and R. Kapral, Phys. Rev. E **52**, 4724 (1995).
[29] D. Horváth and K. Showalter, J. Chem. Phys. **102**, 2471 (1995).
[30] D. Horváth and A. Tóth, J. Chem. Phys. **102**, 2471 (1995).
[31] A. Tóth, I. Lagzi, and D. Horváth, J. Phys. Chem. **100**, 14837 (1996).
[32] A. Tóth, B. Veisz, and D. Horváth, J. Phys. Chem. A **102**, 5157 (1998).
[33] D. Horváth and A. Tóth, J. Chem. Phys. **108**, 1447 (1998).
[34] M. Fuentes, M. N. Kuperman, and P. De Kepper, J. Phys. Chem. A **105**, 6769 (2001).
[35] J. H. Merkin and I. Z. Kiss, Phys. Rev. E **72**, 026219 (2005).
[36] J. H. Merkin and H. Ševčíková, Phys. Chem. Chem. Phys. **1**, 91 (1999).
[37] J. Yang, A. D'Onofrio, S. Kalliadasis, and A. De Wit, J. Chem. Phys. **117**, 9395 (2002).
[38] D. Lima, A. D'Onofrio, and A. De Wit, J. Chem. Phys. **124**, 014509 (2006).
[39] J. D'Hernoncourt, A. De Wit, and A. Zebib, J. Fluid Mech. **576**, 445 (2007).
[40] J. D'Hernoncourt, A. Zebib, and A. De Wit, Phys. Rev. Lett. **96**, 154501 (2006).
[41] J. D'Hernoncourt, J. H. Merkin, and A. De Wit, Phys. Rev. E **76**, 035301 (2007).
[42] J. Yuan, Y. Ju, and C. K. Law, Combust. Flame **144**, 386 (2006).
[43] J. D'Hernoncourt, J. Merkin, and A. De Wit, J. Chem. Phys. **130**, 114503 (2009).
[44] A. B. Tayler, *Mathematical Models in Applied Mechanics* (Oxford Applied Mathematics and Computing Science Series, Clarendon Press, Oxford, 1986).
[45] J. Billingham and D. J. Needham, Philos. Trans. R. Soc. London, Ser. A **334**, 1 (1991).
[46] J. Billingham and D. J. Needham, Dyn. Stab. Syst. **6**, 33 (1991).
[47] J. D'Hernoncourt, J. Merkin, and A. De Wit, J. Chem. Phys. **126**, 104504 (2007).
[48] A. De Wit, Phys. Rev. Lett. **87**, 054502 (2001).
[49] D. A. Vasquez, J. W. Wilder, and B. F. Edwards, J. Chem. Phys. **104**, 9926 (1996).
[50] M. Garbey, A. Taik, and V. Volpert, Q. Appl. Math. **56**, 1 (1998).
[51] B. McCaughey, J. A. Pojman, and C. Simmons, Chaos **8**, 520 (1998).
[52] Y. Wu, D. A. Vasquez, B. F. Edwards, and J. W. Wilder, Phys. Rev. E **51**, 1119 (1995).
[53] Numerical Algorithms Group, Web address: http://www.nag.co.uk/.